Cryogenics 112 (2020) 103121

Contents lists available at ScienceDirect

Cryogenics

journal homepage: www.elsevier.com/locate/cryogenics

Research paper

Adsorption equilibrium and charge/discharge characteristics of hydrogen on MOFs

Zhang Xuan, Zheng Qingrong*, Zhao Guobin, Zhang Weidong

Provincial Key Laboratory of Naval Architecture & Ocean Engineering, Institute of Marine Engineering, Jimei University, Xiamen 361021, China

ARTICLE INFO

Keywords:
MIL-101(Cr)
Adsorption equilibrium
Charge and discharge tests
Hydrogen

ABSTRACT

For obtaining relevant information about the development of hydrogen storage materials from metal organic frameworks (MOFs), MIL-101(Cr) was selected and synthesized for analyzing the adsorption equilibrium and characteristics of charge and discharge. The specific surface area, pore size distribution (PSD) of the sample were determined by 77.15 K nitrogen adsorption data. Isotherms of hydrogen adsorption on the sample were volumetrically measured at 77.15 K and 87.15 K, 0–100 KPa and 0–6 MPa. Henry law constants and Toth equation were respectively used to determine the isosteric heat of adsorption. A 3.2 L conformable vessel, which can meet the fuel consumption of 7.5 kW PEMFC under typical working condition for about 10 min, was designed and undergone charge and discharge tests at ambient temperature and 77.15 K under the flow rate 10–50 L·min^{-1}. Results show that the limit isosteric heat of adsorption on the sample is 7.368 kJ·mol^{-1}, while the mean Isosteric heat determined by the Toth potential function is 2.925 kJ·mol^{-1}. Results also reveal that, at 77.15 K, the ratio of hydrogen released is 80%, 79.4%, 77.2% and 76.1% at the flow rate of 20–50 L·min^{-1}; while at 301.15 K, the ratio is 85.1%, 85.0% and 82.3% with corresponding flow rate 10–30 L·min^{-1}. It suggests that the storage amount and the characteristics of charge/discharge on hydrogen-MIL-101(Cr) system at cryogenic temperature can meet the fuel requirements of the fuel cell.

1. Introduction

Hydrogen energy, which has received wide attention in the world, is a kind of rich resource with an extremely high gravimetric energy density. The effective development and utilization of hydrogen energy are still facing technical problems in such areas as hydrogen production, storage and energy conversion. As one of crucial links in the utilization of hydrogen energy, the storage system is required to be safe, high energy density, low cost and easy to handle [1]. As per the guidelines set by the Department of Energy (DOE) of the United States, the gravimetric storage density of the system is required to meet the target of 4.5 wt% by 2020, 5.5 wt% in 2025 and 6.5 wt% in the final goal at temperature 233.15–358.15 K [2].

At present, there are three main hydrogen storage methods which include high pressure hydrogen storage, liquid hydrogen storage and hydrogen storage on solid materials [3]. However, application of these methods is still limited while taking into account of energy densities, safeties and efficiencies. Physical adsorption of hydrogen has been considered as a promising method for hydrogen storage since 1980s [4], and the relevant researches have greatly been emphasized since Yaghi et al published hydrogen adsorption data on a kind of metal organic frameworks (MOFs) in 1999 [5]. MOFs have the characteristics of high surface area, pore volume, adjustable structure and thermal stability which are crucial to the storage capacity of physical adsorption [6]. Till now, due to much simpler synthesis processes and easier in mass production together with their considerable amounts of adsorption of hydrogen at 77.15 K under a moderate pressure (about 40 bar), comprehensive researches on three kinds of MOFs, viz, MOF-5, MOF-177 and MIL-101(Cr) have been carried out by the main research groups [7], and the MIL-101(Cr) which was firstly synthesized by Ferey group shows better performance on structural stability while forming the composite material [8]. So far, researches of hydrogen adsorption on MOFs have been conducted on such aspects as molecular simulation, structure optimization, charge/discharge test as well as numerical simulation [7], research consensus already achieved can be summarized as follows: (1) The specific surface area, pore volume and crystal density of MOFs are crucial parameters affecting their hydrogen storage capacities [9]; (2) MOFs with high specific surface area and micro-pore volume may have equivalent gravimetric density of hydrogen storage comparable to DOE standard. Increasing the volumetric storage density of MOFs requires a larger crystal density of MOFs [10]; (3) In numerical simulation, the accuracy of the model verified by small-scale test should

* Corresponding author. Tel.: +86 592 6183533; fax: +86 592 6180332.
E-mail address: qrzheng816@sina.com (Q. Zheng).

https://doi.org/10.1016/j.cryogenics.2020.103121
Received 7 February 2020; Received in revised form 26 May 2020; Accepted 18 June 2020
Available online 24 June 2020

be improved to predict the performance and dynamic characteristics of MOFs hydrogen storage system [11,12]; (4) The tank structure should be optimized by considering the balance between storage amount from adsorption equilibrium and that from dynamic storage process of hydrogen [12,13]; (5) The contribution of pore volume is more important than specific surface area for hydrogen adsorption on MOFs [14,15]. Moreover, in the viewpoint of practical application, the structural stability of MOFs should also be highly concerned at the same time.

In this paper, adsorption equilibrium and charge/discharge tests of hydrogen were carried out on the similar test rig and the MIL-101(Cr) to those in our previous study [16]. Volumetric method and a conformable vessel were also employed, adsorption equilibrium measurements and charge/discharge tests were respectively conducted at temperature 77.15–87.15 K, ambient and 77.15 K. Analysis of adsorption equilibrium and dynamic characteristics of charge/discharge were performed in terms of isosteric heat of hydrogen adsorption, temperature fluctuation of the adsorbent bed as well as the accumulated charge/discharge amount.

2. Materials and methods

2.1. Preparation and characterization of MIL-101 sample

MIL-101(Cr) samples were prepared in soft conditions without hydrofluoric acidy by hydrothermal method and activated by soxhlet extraction method quite similar to that mentioned in the literature [17]. 18 g $Cr(NO_3)_3{\cdot}9H_2O$ and 7.38 g H_2BDC were fully dissolved in 225 mL of deionized water under ultrasonic shaking and heated in a 300 mL stainless steel autoclave lined with polytetrafluoroethylene for 18 h at 220 °C. The resulted green solution was extracted by Soxhlet's method in ethanol; the green precipitate was washed twice with DMF at 60 °C for 12 hs. The residual DMF was finally removed by washing twice with anhydrous ethanol.

The SEM images of the synthesized sample are shown in Fig. 1. It seems that the prepared sample has integral crystal surfaces having an average crystal size about 0.5–1 μm. The thermal stability of the sample was studied via thermogravimetric analysis (TGA) and the results are shown in Fig. 2. It shows that the weight loss diagram of the sample has two steps which are similar to that of the literature [18]. As mentioned in literature [16], it can be concluded that the first two steps of the weight loss from 40 °C to 80 °C and from 320 °C to 400 °C could be attributed to the loss of guest water molecules released from the cages.

Adsorption and desorption isotherms of nitrogen at 77.15 K on the sample were measured by employing Micromeritics 3flex, and the desorption data were then used to determine the pore size distribution (PSD) of the sample through non-local density functional theory calculation. It can be seen from Fig. 3, the pores of the MIL-101(Cr) sample are mostly concentrated at 0.74 nm, which suggests a possible potential for hydrogen storage. As shown in Table 1, the BET specific surface area of the MIL-101(Cr) is about 2846 $m^2{\cdot}g^{-1}$.

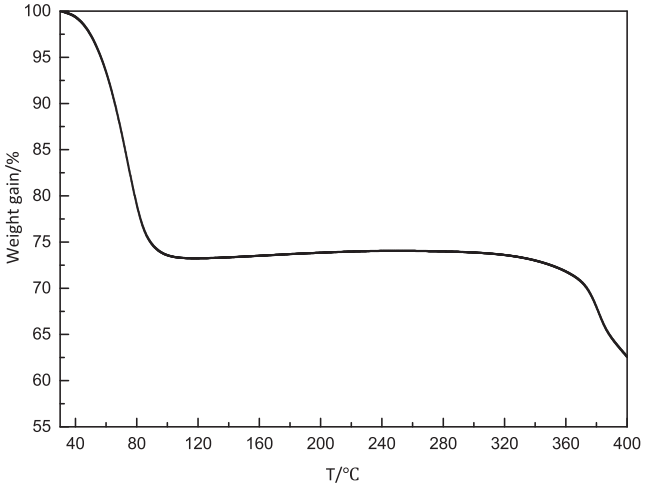

Fig. 2. The results from thermogravimetric analysis of the MIL-101(Cr) sample.

2.2. Measurement of adsorption isotherms

Thinking about that the isosteric heat of adsorption is a crucial parameter for analyzing adsorption equilibrium, isosteric heat at zero surface coverage and that within the experimental condition are expected to accurately determine by adsorption data.

About 0.076 g sample were used while employing Micromeritics 3flex to measure isotherms of hydrogen adsorption on the sample at temperature 77.15 K (liquid nitrogen) and 87.15 K (liquid argon) within pressure 0–0.1 MPa, results are shown in Fig. 4(a). Measuring of adsorption isotherm of hydrogen on the sample (about 0.4413 g in weight) at 77.15 K within pressure range 0–6 MPa was performed on Setaram PCT Pro E&E gas adsorption analyzer. To ensure the accuracy of the experimental data, tests were repeatedly conducted four times and the mean value of the equilibrium data was used to calculate the adsorption isotherm, more information about the experiment has been described in elsewhere [16]. As those shown in Fig. 4(b), within the pressure range 0–6 MPa, it notes that the prepared sample had a maximum excess amount of hydrogen adsorption about 17.892 $mmol{\cdot}g^{-1}$, which is equivalent to the gravimetric density of hydrogen storage 3.89 wt%.

2.3. Charge and discharge tests

In consideration of that the fuel consumption of 7.5 kW PEMFC electrical propulsion plant at different working conditions is equivalent to the flow rate 10–30 $L{\cdot}min^{-1}$ of hydrogen at ambient temperature and 20–50 $L{\cdot}min^{-1}$ at 77.15 K, a conformable vessel which can continuously supply enough hydrogen to the PEMFC for 10 min was designed for charge and discharge tests. The vessel whose structure is

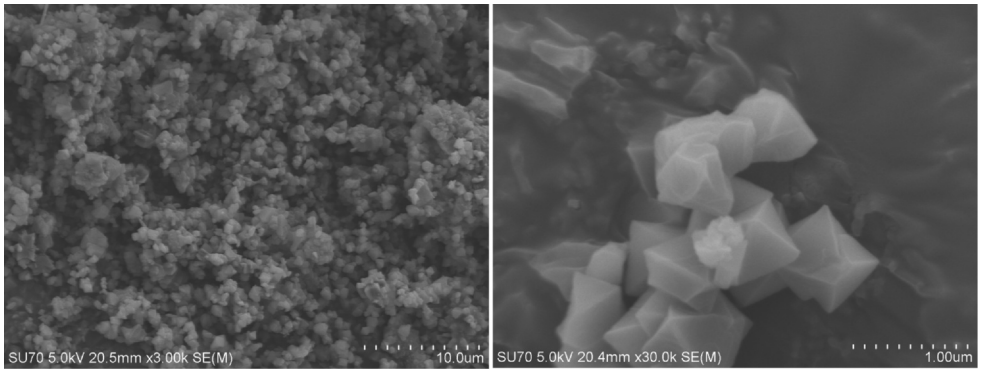

Fig. 1. SEM images of the prepared MIL-101(Cr) sample.

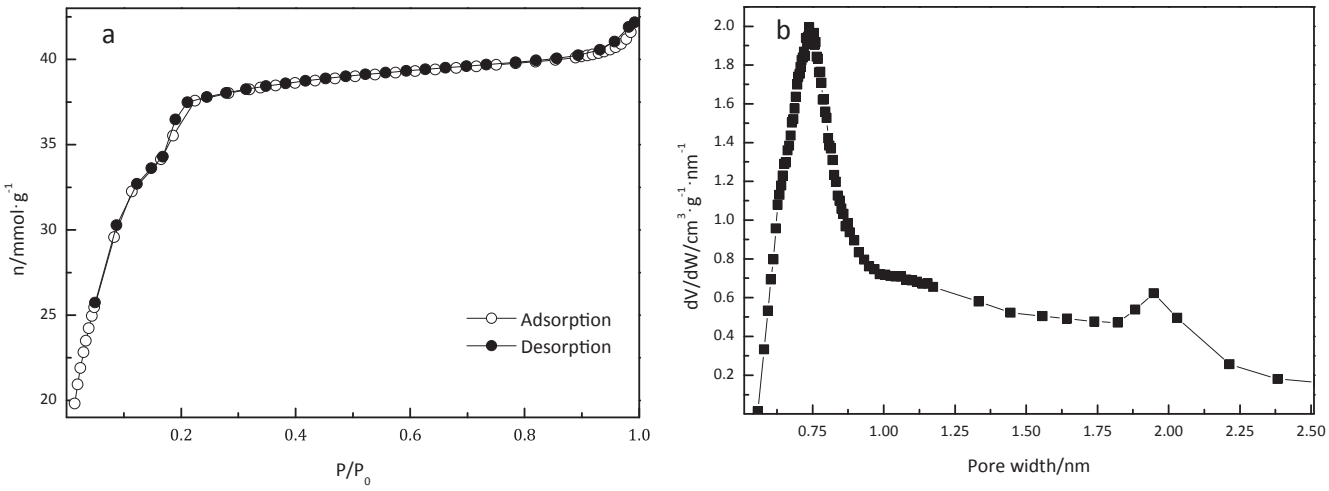

Fig. 3. Isotherms (a) of nitrogen at 77.15 K on MIL-101(Cr) and its PSD (b).

Table 1
Structural parameters of the synthesized the MIL-101(Cr) sample.

Sample	$S_{BET}/m^2 \cdot g^{-1}$	Mean pore width/nm	Micro-pore volume/$cm^3 \cdot g^{-1}$
MIL-101(Cr)	2846	1.8923	0.9495

shown in Fig. 5 has a net volume about 3.2 L, about 950 g MIL-101 sample was packed into the vessel.

The test rig is shown in Fig. 6. Prior to experiments, the system was undergone a leakage test. High purity nitrogen gas at pressure of 15 MPa was used for leakage test, and the air tightness of the system is considered to be feasible while the change of the system pressure is less than 0.2% within 24 h.

3. Results and discussions

3.1. Adsorption equilibrium

It can be seen from Fig. 4(a) that, at low pressure range, adsorption isotherm of hydrogen on the prepared MIL-101 sample conforms to Henry's law [19], that's

$$n = H_P \cdot P, \tag{1}$$

where H_P is Henry's law constant. The limit isosteric heat of adsorption can be determined at the test temperature by linear plotting of the data in Fig. 4(a), and its value can be determined by

$$q_{st0} = RT + R\left(\frac{d\ln H_P}{d\left(\frac{1}{T}\right)}\right), \tag{2}$$

where R is the gas constant, with the value of 8.314 J·(mol·K)$^{-1}$. H_P and the limit isosteric heat of adsorption q_{st0} are shown in Table 2.

As the instrument used in high pressure adsorption test is based on the principle of static volumetric method, the adsorption amount of hydrogen measured on the MIL-101(Cr) is excess amount, but the absolute adsorption amount is generally used in practical application. Therefore, it is necessary to convert the excess adsorption amount into absolute adsorption amount.

According to Gibbs' definition of adsorption [20], one can have the following expression as

$$n_{exc} = n_{abs} - v_a \cdot \rho_g = v_a \cdot \rho_a - v_a \cdot \rho_g = n_{abs}\left(1 - \frac{\rho_g}{\rho_a}\right). \tag{3}$$

Here, n_{exc} is the excess amount of adsorption; n_{abs} the absolute amount; ρ_a the density of the adsorbed phase; v_a the specific volume of the adsorbed phase. Here, ρ_g of hydrogen is determined by the 32 parameter MBWR equation [21].

Thinking about that the absolute adsorption amount is more meaningful for practical application, here, Toth equation is used for model study, that's [22],

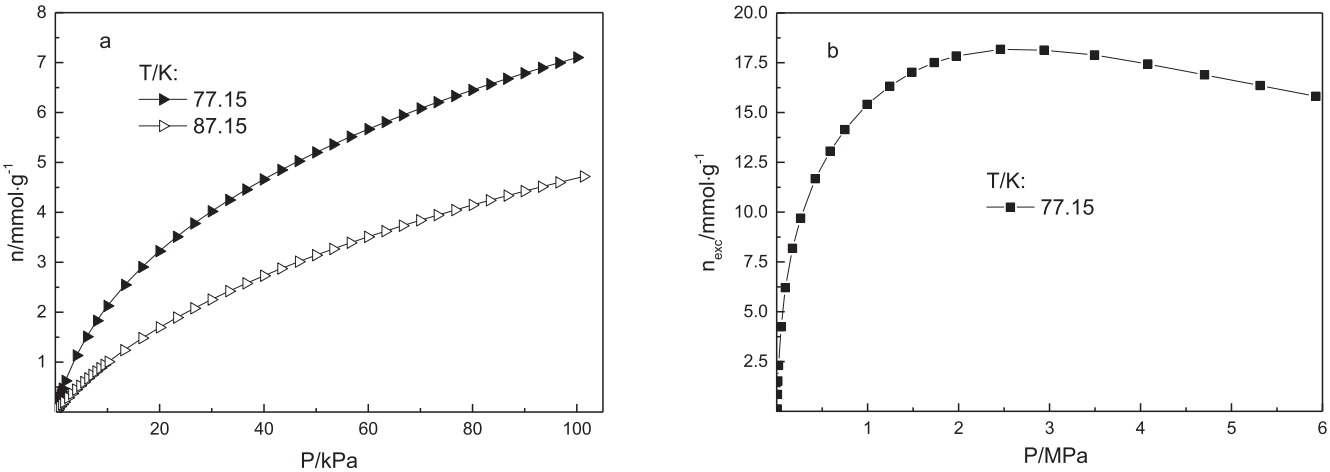

Fig. 4. Isotherms of hydrogen adsorption on MIL-101(Cr) at low pressure (a) and high pressure (b).

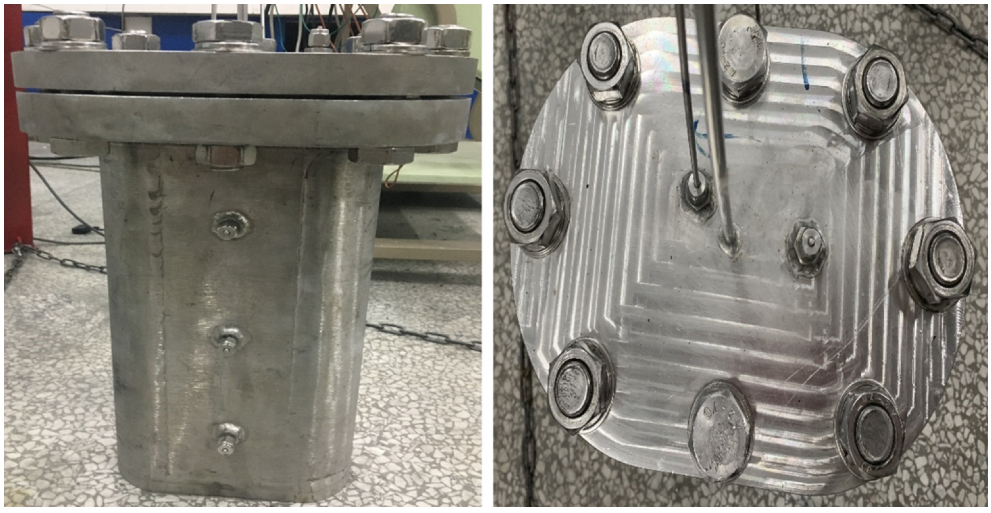

Fig. 5. Structure of a conformable tank.

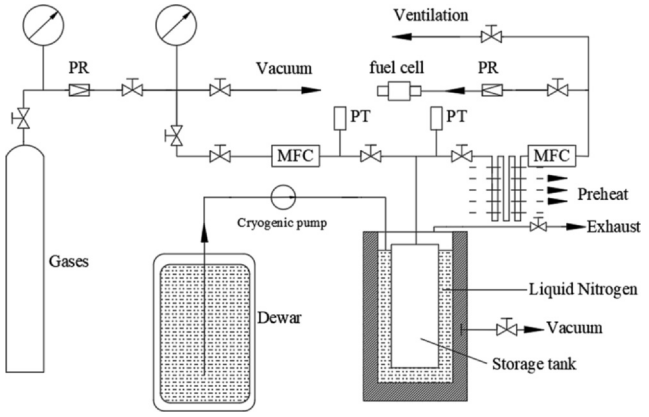

Fig. 6. Schematic diagram of charge and discharge experimental unit.

Table 2
Thermodynamic parameters of hydrogen adsorption on MIL-101(Cr) sample.

T/K	H_P/mmol·Pa^{-1}·g^{-1}	q_{st0}/kJ·mol^{-1}	Mean limit isosteric heat/kJ·mol^{-1}
77.15	3.85E-04	7.326	7.368
87.15	1.16E-04	7.409	

$$n_{abs} = n_m \frac{bf}{[1 + (bf)^t]^{1/t}}. \quad (4)$$

Here, n_m is the saturation adsorption capacity; f the bulk gas fugacity; b and t parameters which can be nonlinearly determined by fitting the experimental data from Eq. (3). The mean deviation δ is used to evaluate the accuracy of fitting, that's

$$\delta = \frac{1}{N}\sum_{i=1}^{N}\frac{|n_{exc}^i - n_{cal}^i|}{n_{exc}^i} \times 100\%, \quad (5)$$

Isosteric heat of adsorption can be determined by Toth potential function [23],

$$q_{st} = RT\ln\left(\frac{P_s}{P} \times (bP)^t\right) + \lambda + zRT, \quad (6)$$

$$P_S = P_C\left(\frac{T}{T_C}\right)^2. \quad (7)$$

where P_C is the critical pressure; λ the latent heat of vaporization, which is about 0.92 kJ·mol^{-1} for hydrogen [23]; $z$the compressibility factor, which can be obtained by SRK equation [24]; $b$and t the parameters in the Toth equation. Values of the parameters determined by nonlinearly fitting are shown in Table 3. It suggests that Toth equation can much accurately predict the adsorption amount with a mean relative deviation about 0.167%. Comparisons among the absolute amount and excess amounts are shown in Fig. 7a, and the isosteric heat of hydrogen adsorption on the sample accordingly determined is shown in Fig. 7b.

Table 3
Values of fitting parameters by Toth Equation.

Sample	n_m/mmol·g^{-1}	b/MPa^{-1}	t	δ/%
MIL-101(Cr)	53.98	4.791	0.3911	0.167

As it can be seen from Fig. 7(a), at 77.15 K, the excess adsorption amount obtains its maximum about 17.892 mmol·g^{-1} at pressure 2.94 MPa, while that of hydrogen on the activated carbon AX-21 having a specific surface area about 2800 m^2·g^{-1} reached its maximum about 26.75 mmol·g^{-1} at pressure about 3.6 MPa [25]. It is noted in Fig. 7(b), that the isosteric heats of adsorption on the sample decreases from 4.18 to 1.67 kJ·mol^{-1} in comparing with 6.4 to 5.0 kJ·mol^{-1} of hydrogen on the activated carbon AX-21[25], which suggests that adsorption performance of hydrogen on the prepared MIL-101(Cr) sample is weaker than that on the activated carbon AX-21.

3.2. Analysis of charging and discharging process

3.2.1. Charge/ discharge at ambient temperature

Figs. 8 and 9 show temperature records at the central region and the wall of the storage vessel while charging and discharging the storage vessel with a flow rate from 10 L·min^{-1} to 30 L·min^{-1}.

It can be seen from Fig. 8 that, when the charging flow rate increases, the temperature at both the central region and wall increases, the corresponding time to reach their maximums decreases, which accordingly results in an increase in the average temperature of the tank. The larger the flow rate of charge, the shorter the duration for the temperatures to reach their maximums, which in return causes a larger fluctuation of the temperature. While charging at flow rate 10 L·min^{-1}, 20 L·min^{-1} and 30 L·min^{-1}, within the duration about 1500 s when the temperatures seem to be stable, the storage tank can respectively have an average temperature rise about 5 °C, 8 °C and 9 °C, which are in correspondence with the amount of charge about 4.22 g, 4.03 g and 3.96 g. This suggests that, at temperature 301.15 K and under pressure 7.2 MPa, the charged amount can be increased while a smaller flow rate

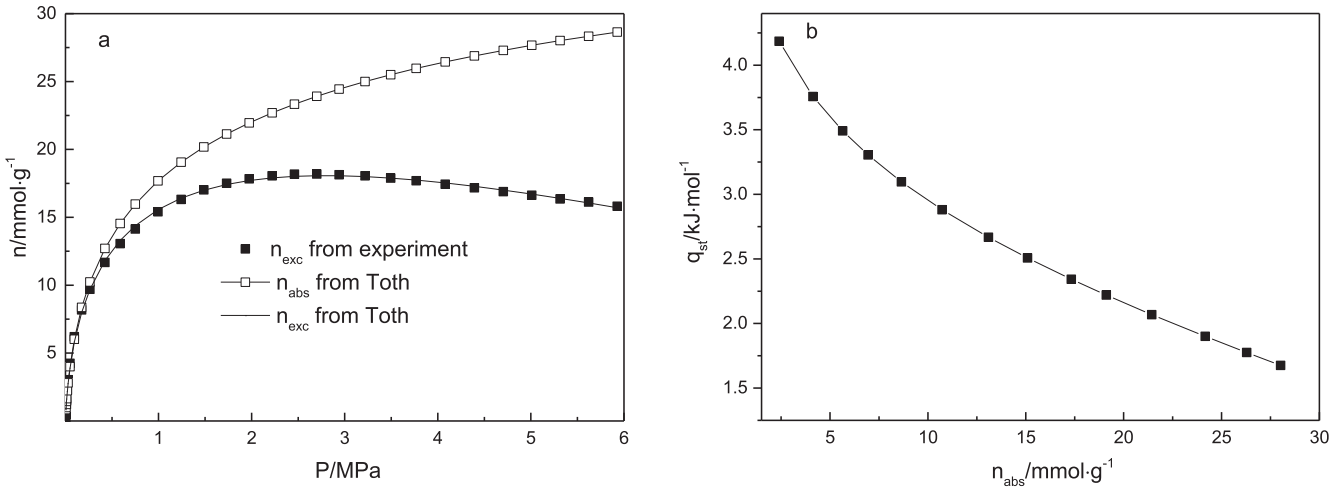

Fig. 7. Isotherms (a) and isosteric heat (b) of hydrogen adsorption on MIL-101(Cr).

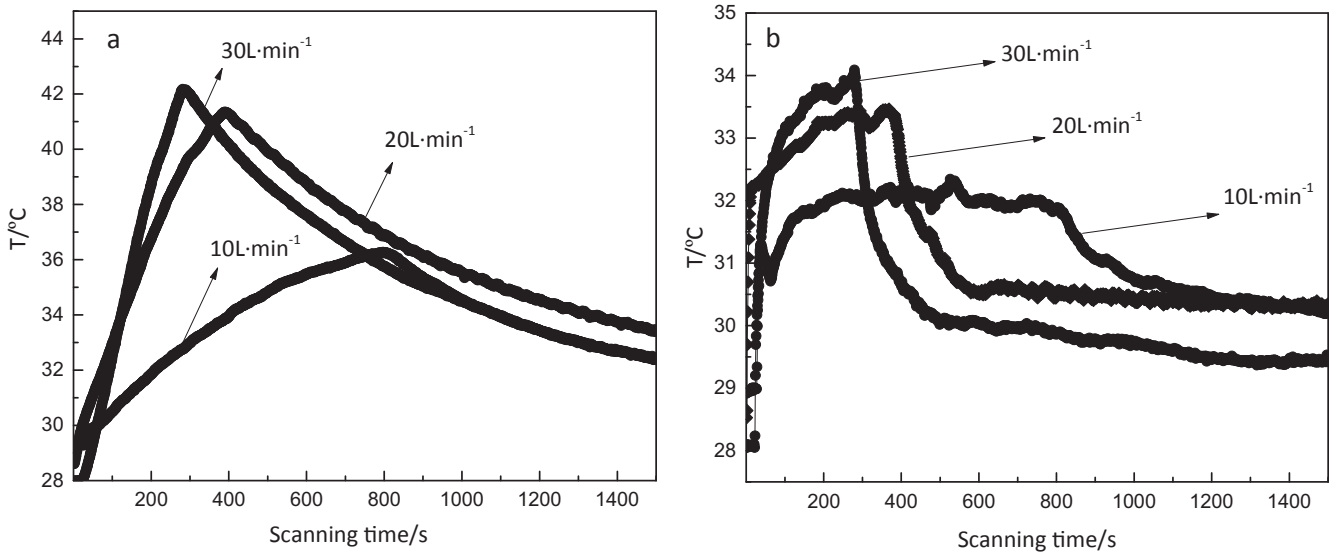

Fig. 8. Variations of temperature at the central region and the wall of the storage vessel during the charge..

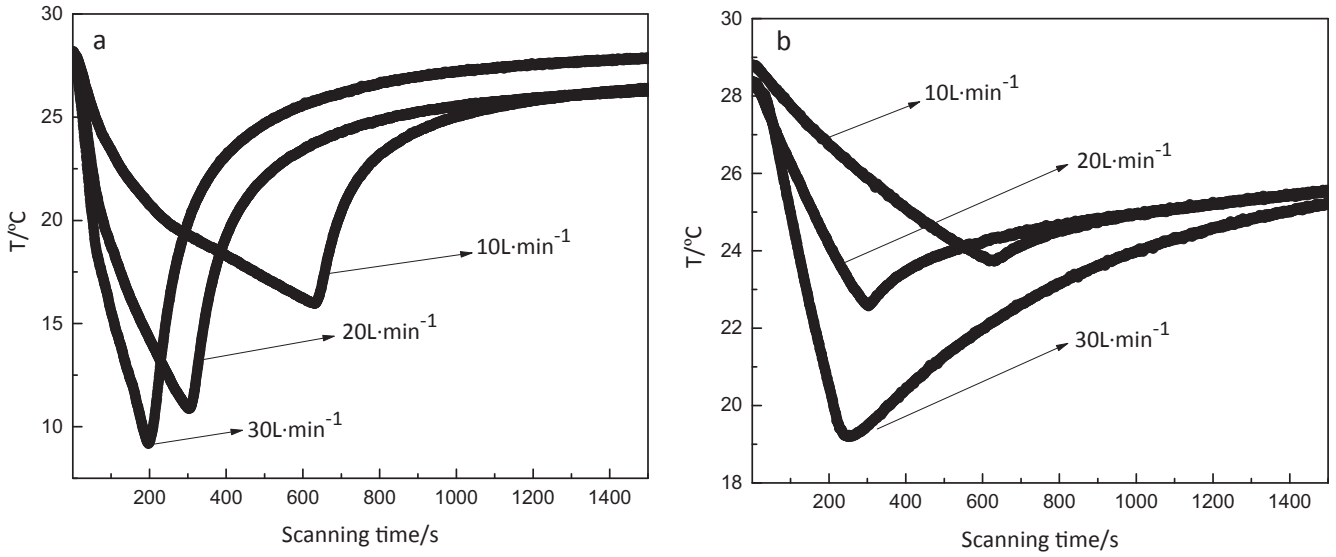

Fig. 9. Variations of temperature at the central region and the wall of the storage vessel during the discharge.

Table 4
Parameters at different flow rates of charge and discharge at ambient temperature.

Flow rate/L·min^{-1}	T_{max}/°C	T_{min}/°C	$T_{\triangle}$/°C	Usable capacity ratio(UCR) determined by discharge and charge amount/%
10	36	16	7/12	85.1
20	41	13	13/16	85.0
30	42	10	14/20	82.3

Notes: T_{max} is the highest temperature at the central region of the vessel during charging process; T_{min} is the lowest temperature at the central region of the vessel during the discharging process; $T_{\triangle}$ is the increase/decrease of temperature between the central region and the wall of the vessel during the charge/discharge.

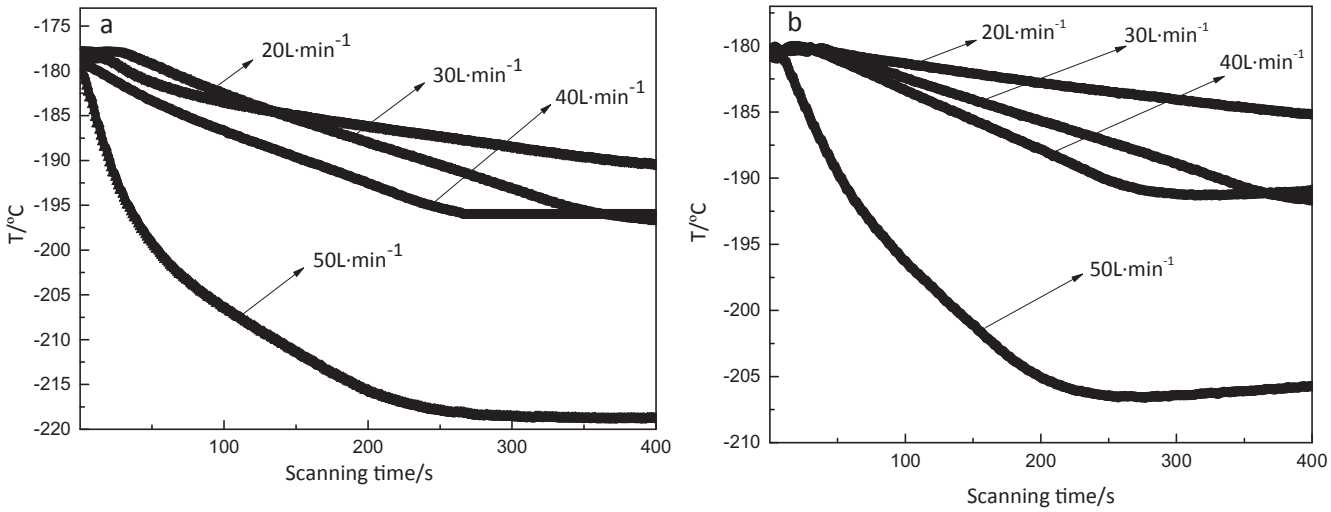

Fig. 10. Variations of temperature at the central region (a) and the wall (b) of the storage vessel during the discharge at different flow rates.

Table 5
Various parameters at different flow rates at discharge.

Flow rate of discharge/L·min^{-1}	T_{min}/°C	$T_{\triangle}$/°C	Usable capacity ratio(UCR) determined by discharge and charge amount/%
20	−195	17 /7	80.0
30	−196	18/10	79.4
40	−198	20/12	77.2
50	−218	41/26	76.1

Notes: T_{min} is the minimum temperature at the central region of the storage vessel during the discharge; T_{Δ} is the temperature drop at the central region/wall of the storage vessel in the process of discharge.

is employed. This argument is consistent with the conclusion drawn in our previous study [16], that's, while a larger flow rate was employed, the contribution from the heat of compression among gas molecules may become greater and accordingly cut down the total amount of charge.

As noted in Fig. 9, temperature variation curves at the central region and the wall of the storage vessel get gentler while a smaller flow rate of discharge is used, that's, a smaller flow rate of discharge obviously cut down the amplitude of temperature change and prolong the process for reaching the lowest value of the temperature. It can be seen from Fig. 9(a) and (b) that, when the discharging flow rate increased from 10 L·min^{-1} to 30 L·min^{-1}, the average temperature of the storage vessel decreased by 12 °C in the duration about 1500 s. It can also be found that, under the flow rate of 10–30 L·min^{-1}, within the effective discharge duration (here, this duration is denoted as the duration from the initial of the discharge to that where the temperature at the central region is similar to that of the environment), the total amount of discharge accumulated by MFC is respectively about 3.59 g, 3.49 g and 3.26 g, which is in correspondence with the ratio of discharge about 85.1%, 85% and 82.3%. Actually, this phenomenon can be ascribed to a larger drop of the temperature at the storage vessel while discharging at a larger flow rate. Comprehensive comparisons shown in Table 4 reveal that, within the effective charge/discharge duration, not only can a smaller flow rate effectively inhibit the temperature fluctuation of the storage system, it can also be beneficial to increasing its usable capacity ratio (UCR). Thinking about that the flow rate should meet the requirement of the fuel consumption of the power system, and a certain flow rate is always needed for practical application, it is therefore a necessity to equip thermal effect management measures for balancing the heat gain and heat loss in charging and discharging process.

3.2.2. Discharge at low temperatures

Discharge tests were conducted while the liquid nitrogen had been withdrawn from the cooling space of the storage vessel. As those shown in Fig. 10 and Table 5, similar to the results obtained from the tests performed at ambient temperature, a smaller flow rate of discharge is beneficial to weakening the thermal effect on the storage vessel in terms of reducing the fluctuation amplitude of the temperature as well as increasing the amount of discharge within an effective period.

It can be found that, under the flow rate 20 L·min^{-1}, in comparing with 16 °C and 7 °C temperature decrement at the central region and the wall of the storage vessel, there are correspondingly about 41 °C and 26 °C under flow rate 50 L·min^{-1}, which accordingly cut down the UCR from 80.0% to 76.1%. It suggests that, the flow rate of discharge should also be carefully selected since the stability of the temperature of the storage system is more sensible to heat under cryogenic environment than that at ambient temperature. In the viewpoint of practical application, prior to leading to the fuel cell stack, hydrogen released from the storage vessel at low temperature should be preheated in a preheater or a buffer tank, a smaller flow rate can therefore be selected by optimization match among the heat conducting enhancement of the storage system, the structure of the storage vessel and the hydrogen consumption rate of the fuel cell stack.

The effect of temperature on the adsorptive performance of the storage vessel is obviously. As those shown in Fig. 11, at the flow rate of

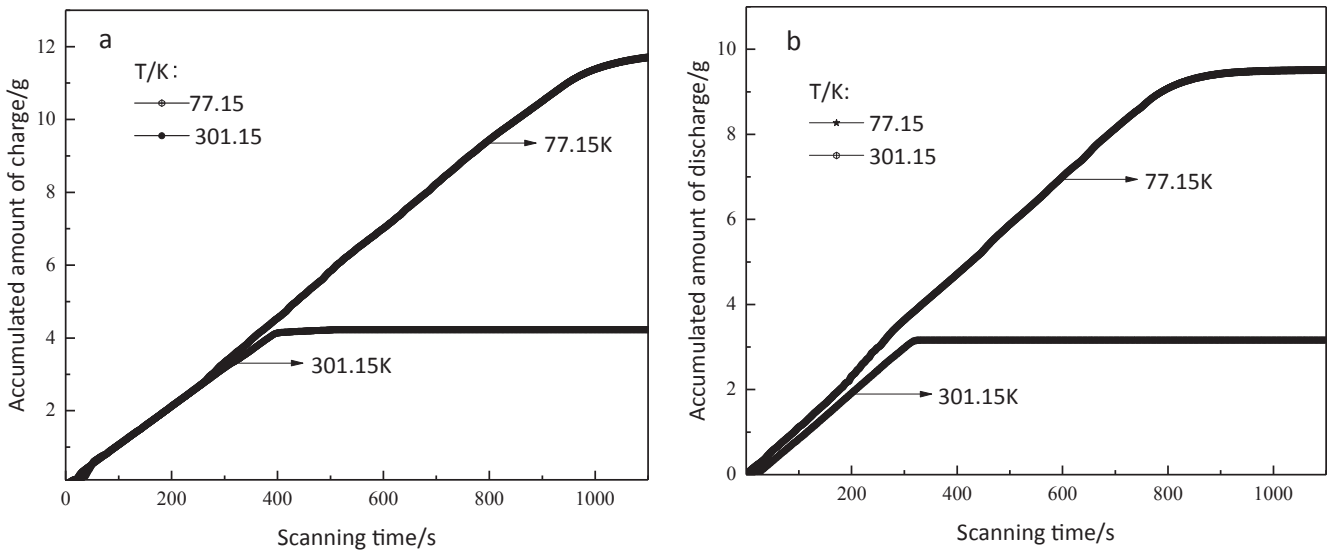

Fig. 11. Amount of charge (a) and discharge (b) under flow rate 20 L·min^{-1} at ambient temperature and low temperature.

20 L·min^{-1}, the total amount of charge at 77.15 K is 11.89 g in comparing with 4.03 g at 301.15 K, and that of discharge at 77.15 K and 301.15 K is about 9.51 g and 3.15 g. It is clear that both the charge and discharge amounts have nearly been tripled while decreasing the temperature of the storage system from 301.15 K to 77.15 K. Another important characteristic can be found in Fig. 11, that the effective charge duration is about 400 s at 301.15 K and 1100 s at 77.15 K, while that for discharge is 350 s at 301.15 K and 950 s at 77.15 K. It suggests that the increasing/decreasing rate of the amount of hydrogen confined within the storage vessel is nearly independent of the temperature of the storage system, which means that the thermal conductivity of the as-prepared MIL-101(Cr) can be considered as temperature independent. It is therefore a need to equip heat conducting enhancement measures for H_2-MOFs storage system used under low temperature.

4. Conclusions

(1) At temperature 77.15 K and 87.15 K, the isosteric heat of hydrogen adsorption on the synthesized MIL-101 (Cr) sample is about 1.67–7.368 kJ·mol^{-1}. The prepared MIL-101(Cr) sample has a specific surface area, micro-pore volume respectively about 2846 m^2·g^{-1} and 0.9495 cm^3·g^{-1}, the maximum hydrogen storage capacity of 0–6 MPa is 17.892 mmol·g^{-1}, which is equivalent to the gravimetric density of hydrogen 3.89 wt%.

(2) The setting of the flow rate for charging/discharging the storage vessel is crucial to the charge/discharge amount. While conducting the charge and discharge at ambient temperature, a larger flow rate of charge/discharge brings about a stronger fluctuation of the temperature of the storage vessel, which accordingly cut down the amount of charge/discharge. It suggests that a smaller flow rate should be employed for charge and discharge to mitigate the temperature fluctuation of the adsorbent bed.

(3) While discharging a storage tank in volume 3.2 L at 77.15 K, mitigating the temperature drop within the initial discharge period about 300 s is crucial to the amount of discharge. It notes that, with the increase of the flow rate of discharge, the ratio of the discharged amount and the temperature of the storage tank respectively gets smaller and drops down to a lower value. It suggests that a smaller flow rate of discharge is also a priority.

(4) The thermal conductivity of the prepared MIL-101(Cr) is temperature independent. Under the same flow rate and the same pressure, the effective charge duration is temperature dependent, lowering down the temperature of the storage system prolongs the effective charge duration, but the increasing rate of the charge amount seems to be temperature independent. It notes that heat conducting enhancement measures is vital to the practical application of cryo-adsorption of hydrogen on MOFs.

Declaration of Competing Interest

The authors declare that they have no known competing financial interests or personal relationships that could have appeared to influence the work reported in this paper.

Acknowledgements

The project was supported by National Natural Science Foundation of China (51979121) P.R. China.

Appendix A. Supplementary material

Supplementary data to this article can be found online at https://doi.org/10.1016/j.cryogenics.2020.103121.

References

[1] Justin P, Mike V, David T, et al. Estimation of system-level hydrogen storage for metal-organic frameworks with high volumetric storage density. Int J Hydrogen Energ 2019;44(29):15135–45.
[2] US DOE targets for onboard hydrogen storage systems for light-duty vehicles. Available at < https://www.energy.gov/eere/fuelcells/doe-technical-targets-onboard-hydrogen-storage-light-duty-vehicles > .
[3] Ramin M, Katrina MG. Hydrogen storage and delivery: review of the state of the art technologies and risk and reliability analysis. Int J Hydrogen Energy 2019;44(23):12254–69.
[4] Sdanghi G, Schaefer S, Maranzana G, Celzard A, Fierro V. Application of the modified Dubinin-Astakhov equation for a better understanding of highpressure hydrogen adsorption on activated carbons, Int J Hydrogen Energy, https://doi.org/10.1016/ j.ijhydene.2019.09.240.
[5] Li HL, Eddaoudi M, O'Keeffe M, Yaghi OM. Design and synthesis of an exceptionally stable and highly porous metal-organic framework. Nature 1999;402(6759):276–9.
[6] Kranthi KG, Suresh M, Saratchandra BM, et al. Characteristics of MOF, MWCNT and graphene containing materials for hydrogen storage: a review. J Energ Chem 2018;15(56):2–3.
[7] Corgnale C, Hardy B, Chahine R, Zacharia R, Cossement D. Hydrogen storage in a two-liter adsorbent prototype tank for fuel cell driven vehicles. Appl Energy 2019;250:333–43.
[8] Yu ZW, Deschamps J, Hamon L, Karikkethu P Prasanth. Pré P. Hydrogen adsorption and kinetics in MIL-101(Cr) and hybrid activated carbon-MIL-101(Cr) materials. Int J Hydrogen Energ 2017;42(12):8021–31.
[9] Antonio ND, Nuno B, Leighton TH, Ibbi YA, Valeska PT, Timothy JM. Structure-property relationships in metal-organic frameworks for hydrogen storage. Colloids

Surf A Physicochem Eng Asp 2016;496:77–85.
[10] Kumar KV, Preuss K, Titirici MM, Rodríguez-Reinoso F. Nanoporous materials for the onboard storage of natural gas. Chem Rev 2017;117(3):1796–825.
[11] Hardy B, Tamburello D, Corgnale C. Hydrogen storage adsorbent systems acceptability envelope. Int J Hydrogen Energ 2018;43(42):19528–39.
[12] Purewal J, Veenstra M, Tamburello D, Ahmed A, Matzger, Adam J, Wong-Foy AG, Seth S, Liu YY, Siegel DJ. Estimation of system-level hydrogen storage for metal-organic frameworks with high volumetric storage density. Int J Hydrogen Energ 2019;44(29):15135–45.
[13] Corgnale C, Hardy B, Chahine R, Cossement D. Hydrogen desorption using honeycomb finned heat exchangers integrated in adsorbent storage systems. Appl Energy 2018;213:426–34.
[14] Broom DP, Webb CJ, Fanourgakis GS, et al. Concepts for improving hydrogen storage in nanoporous materials. Int J Hydrogen Energ 2019;44(15):7768–79.
[15] Balderas-Xicohténcatl R, Schlichtenmayer M, Hirscher M. Volumetric hydrogen storage capacity in metal–organic frameworks. Energy Technol 2018;6(3):578–82.
[16] Zhao GB, Zheng QR, Zhang WD, et al. Adsorption equilibrium and charge/discharge characteristics of methane on MIL-101. J Fuel Chem Technol 2019;47(12):1529–36. (in Chinese).
[17] Bromberg L, Diao Y, Wu HM, et al. Chromium(III) terephthalate metal organic framework (MIL-101):HF-Free synthesis, structure, polyoxometalate composites, and catalytic properties. Chem Mater 2012;24(9):1664–75.
[18] Yu ZW, Deschamps J, Hamon L, et al. Hydrogen adsorption and kinetics in MIL-101(Cr) and hybrid activated carbon-MIL101(Cr) materials. Int J Hydrogen Energ 2017;42(12):8021–31.
[19] Clark A. The theory of adsorption and catalysis. New York: Academic Press; 1970. p. 394–5.
[20] Menon PG. Adsorption at high pressures. Chem Rev 1968;68(3):277–94.
[21] Johnson JK, Zollweg JA, Gubbins KE. The Lennard-Jones equation of state revisited. Mol Phys 1993;78(3):591–618.
[22] Do DD, Do HD. Adsorption of supercritical fluids in non-porous and porous carbons: analysis of adsorbed phase volume and density. Carbon 2003;41(9):1777–91.
[23] Kloutse AF, Zacharia R, Cossement D, et al. Isosteric heat of hydrogen adsorption on MOFs: comparison between adsorption calorimetry, sorption isosteric method, and analytical models. Appl Phys A 2015;121(4):1417–24.
[24] Soave G. Equilibrium constants from a modified Redlich-Kwong equation of state. Chem Eng Sci 1972;27(6):1197–203.
[25] Bénard P, Chahine R. Determination of the adsorption isotherms of hydrogen on activated carbons above the Critical Temperature of the adsorbate over wide temperature and pressure. Langmuir 2001;17(6):1950–5.